Journal of Alloys and Compounds 506 (2010) 475–481

Contents lists available at ScienceDirect

Journal of Alloys and Compounds

journal homepage: www.elsevier.com/locate/jallcom

Luminescence and absorbance of highly crystalline $CaMoO_4$, $SrMoO_4$, $CaWO_4$ and $SrWO_4$ nanoparticles synthesized by co-precipitation method at room temperature

Titipun Thongtem[a,*], Sukjit Kungwankunakorn[a], Budsabong Kuntalue[b], Anukorn Phuruangrat[c,*], Somchai Thongtem[c]

[a] Department of Chemistry, Faculty of Science, Chiang Mai University, Chiang Mai 50200, Thailand
[b] Electron Microscopy Research and Service Center, Faculty of Science, Chiang Mai University, Chiang Mai 50200, Thailand
[c] Department of Physics and Materials Science, Faculty of Science, Chiang Mai University, Chiang Mai 50200, Thailand

ARTICLE INFO

Article history:
Received 12 December 2009
Received in revised form 7 July 2010
Accepted 7 July 2010
Available online 15 July 2010

Keywords:
Nanostructured materials
Co-precipitation
Luminescence
Optical spectroscopy

ABSTRACT

Highly crystalline $CaMoO_4$, $SrMoO_4$, $CaWO_4$ and $SrWO_4$ nanoparticles were successfully synthesized by the co-precipitation of mixtures of $Ca(NO_3)_2{\bullet}4H_2O$ or $Sr(NO_3)_2$, and $Na_2MoO_4{\bullet}2H_2O$ or $Na_2WO_4{\bullet}2H_2O$ dissolved in ethylene glycol at room temperature (30 °C). Phases, morphologies, atomic vibrations and optical properties were analyzed by X-ray diffraction, transmission electron microscopy, Fourier transform infrared and Raman spectrophotometry, and ultraviolet–visible and photoluminescent spectroscopy. All products were proved to be MXO_4 (M = Ca and Sr, and X = Mo and W) with body-centered tetragonal scheelite structures, having round nanoparticles with the average sizes of 12.06 ± 1.65, 16.40 ± 2.44, 15.49 ± 2.19, and 15.40 ± 2.30 nm for $CaMoO_4$, $SrMoO_4$, $CaWO_4$ and $SrWO_4$, respectively. Their $\nu_1(A_g)$, $\nu_3(B_g)$, $\nu_3(E_g)$, $\nu_4(B_g)$, $\nu_2(A_g)$ and $\nu_{f.r.}(A_g)$ vibration modes were also detected – being shifted to lower wavenumbers from $MMoO_4$ to MWO_4, due to the change of efficient atomic mass of the oscillating ions between X^{6+} and O^{2-} in the $[XO_4]^{2-}$ complexes. Band gaps of $CaMoO_4$, $SrMoO_4$, $CaWO_4$ and $SrWO_4$ were determined to be 5.07, 3.72, 5.40, and 4.47 eV, respectively. Photoluminescent (PL) emissions were at 414, 413, 418, and 414 nm for $CaMoO_4$, $SrMoO_4$, $CaWO_4$ and $SrWO_4$, respectively.

1. Introduction

Molybdates and tungstates are important luminescent materials with scheelite-type tetragonal structure, belonging to $I4_1/a$ space group with two formula units per primitive cell. Each of X atoms (X = Mo and W) is surrounded by four equivalent O atoms composing the $[XO_4]^{2-}$ tetrahedral configuration and each divalent metal shares corners with eight adjacent O atoms of $[XO_4]^{2-}$ tetrahedrons [1–5]. Alkaline earth metal molybdates and tungstates are very interesting materials due to their structural properties, great potential and promising applications. $CaMoO_4$ and $SrMoO_4$ have attracted particular interest in a variety of applications such as hosts for lanthanide activated lasers, luminescence materials, microwave applications and catalysts [5–7]. $CaWO_4$ can be used for luminescence, thermoluminescence, stimulated Raman scattering behavior, and superior luminescence as blue phosphor (433 nm) [8]. $CaWO_4$ and $SrWO_4$ have attracted attention for using in oscilloscopes, and as scintillating material for detecting X- and γ-rays in medical applications [8,9].

Nanomaterials have interesting opto-electrical properties which are different from their bulks. These properties are controlled by uniform shape and narrow size distribution [10]. There are a variety of methods used to synthesize metal molybdates and tungstates such as hydrothermal process [11,12], microwave-assisted synthesis [13] and cyclic microwave irradiation [14], microwave-hydrothermal synthesis [2–4,15], and sonochemical method [16]. In a solution system, solvent is important to control dispersion of particles. Specifically, polyol as ethylene glycol (EG) has been widely used for synthesizing of dispersion nanomaterials because the reaction is able to efficiently proceed [16] – EG is one of the efficient absorbers and stabilizers. In this report, we present the synthesis of nanocrystalline alkaline earth metal molybdates and tungstates (M = Ca and Sr) by co-precipitation method at room temperature without the subsequent calcination at high temperature. This method is simple, low energy consumption and friendly to the environment.

2. Experiment

Calcium nitrate tetrahydrate (99% $Ca(NO_3)_2{\bullet}4H_2O$), strontium nitrate (≥99% $Sr(NO_3)_2$), sodium molybdate dihydrate (≥99% $Na_2MoO_4{\bullet}2H_2O$) and sodium tungstate dihydrate (99% $Na_2WO_4{\bullet}2H_2O$) were purchased from Sigma–Aldrich Reagents Co., and used without further purification. Each 0.005 mole of these start-

* Corresponding authors. Tel.: +66 (0)53 943344; fax: +66 (0)53 892277.
E-mail addresses: ttpthongtem@yahoo.com (T. Thongtem), phuruangrat@hotmail.com (A. Phuruangrat).

0925-8388/$ – see front matter © 2010 Elsevier B.V. All rights reserved.
doi:10.1016/j.jallcom.2010.07.033

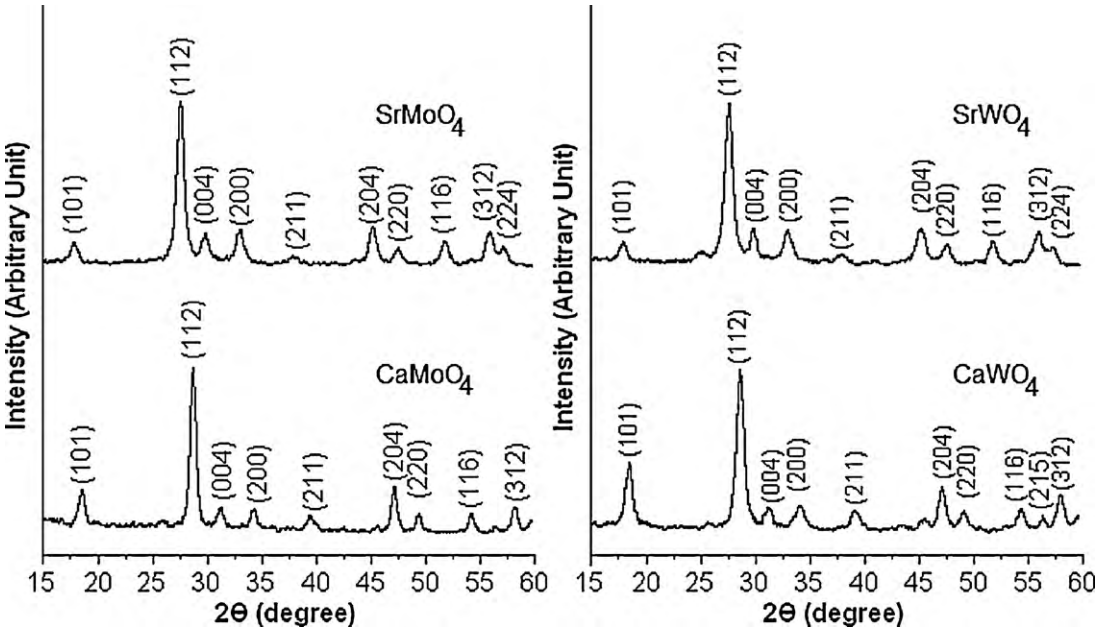

Fig. 1. XRD patterns of $CaMoO_4$, $SrMoO_4$, $CaWO_4$ and $SrWO_4$.

ing materials was separately dissolved in 15.00 mL ethylene glycol, used as a solvent. After the starting materials were completely dissolved, white solutions formed. Then the corresponding two solutions were mixed together with continuous stirring for 24 h at room temperature (30 °C). Finally, white precipitates were synthesized, washed with distilled water and absolute ethanol, and dried in air at 80 °C for 24 h.

Their phases, morphologies, and atomic vibration were characterized by D-500 Siemens X-ray diffractometer (XRD), using Cu K_α radiation, the scanning 2θ angle of 15–60° range, with a graphitic monochromator and a Ni filter, Bruker Tensor 27 Fourier transform infrared (FTIR) spectrometer with diluted KBr, HORIBA JOBIN YVON T64000 Raman spectrometer using 50 mW Ar laser with $\lambda = 514.5$ nm, and JEOL, JEM-2010 transmission electron microscope (TEM) carried out at 200 kV. The samples for TEM analysis were dispersed in ethanol under ultrasonic radiation and the dispersed samples were dropped on the supported carbon film coated on 3-mm diameter fine-mesh copper grids. Their optical properties were recorded by Lambda-25 Perkin-Elmer UV–visible, and LS50B Perkin-Elmer luminescence spectrophotometers.

3. Results and discussion

Fig. 1 shows XRD patterns of alkaline earth metal molybdate and tungstate (M = Ca and Sr) nanocrystals. They show pure phases of body-centered tetragonal system ($a = b \neq c$ and $\alpha = \beta = \gamma = 90°$) for $CaMoO_4$, $SrMoO_4$, $CaWO_4$ and $SrWO_4$ structures with no detection of any impurities, comparing to the JCPDS database nos. 85-0585 ($CaMoO_4$), 85-0586 ($SrMoO_4$), 41-1431 ($CaWO_4$) and 85-0587 ($SrWO_4$) [1,17]. $M(NO_3)_2{\bullet}xH_2O$ (M = Ca for $x = 4$, and M = Sr for $x = 0$) and $Na_2XO_4{\bullet}2H_2O$ (X = Mo, W), separately dissolved in ethylene glycol, were mixed and stirred for 24 h at room temperature, to form MXO_4 (white precipitates) by the following reaction.

$$M(NO_3)_2 \cdot xH_2O + Na_2XO_4 \cdot 2H_2O \xrightarrow{\text{in EG, 24 h stirring}} MXO_4 + 2NaNO_3 + (x+2)H_2O \quad (1)$$

Their lattice parameters were calculated from the plane-spacing equation for tetragonal structure and Bragg's law for diffraction [18] – summarized in Table 1 and very close to their corresponding standard values [17]. The increase of lattice parameters from $CaMoO_4$ to $SrMoO_4$, and $CaWO_4$ to $SrWO_4$ is related to ionic radii of alkaline earth metals ($Ca^{2+} = 1.12$ Å and $Sr^{2+} = 1.25$ Å) [1]. For scheelite structure, each of X (X = Mo and W) ions is in the tetrahedrons of O ions, and the divalent M (M = Ca and Sr) ions are surrounded by eight O ions [1,5,19]. Their approximate crystallite sizes were calculated from the (1 1 2) peaks of their corresponding XRD patterns and Scherrer's equation [18,20], as shown below.

$$L = \frac{\lambda k}{B \cos\theta} \quad (2)$$

The λ, θ, k, and B parameters are the wavelength of Cu K_α radiation (1.54056 Å) [21], Bragg angle of the (1 1 2) planes, a constant (0.89), and full width at half maximum of the (1 1 2) peaks in radian. Their approximate crystallite sizes are 14, 17, 18 and 20 nm for $CaMoO_4$, $SrMoO_4$, $CaWO_4$ and $SrWO_4$, respectively.

In the solution system, the MXO_4 (M = Ca and Sr, X = Mo and W) nanoparticles precipitated – M^{2+} cations as electron pair acceptors (Lewis acid) reacted with XO_4^{2-} anions as electron pair donors (Lewis base). The reaction between these two species ($M^{2+} \leftarrow :XO_4^{2-}$) proceeded to produce bonding. The lowest molecular orbital energy of Lewis acid interacted with the highest molecular orbital energy of Lewis base, and MXO_4 nanoparticles were finally synthesized [4,15].

Scheelite structure has $[XO_4]^{2-}$ molecular ionic units with strong X–O covalent bonds, which have weak coupling with M^{2+} cations. Group theory calculation presents 26 different vibrations for MXO_4 crystal with zero wavevector ($\vec{k} = \vec{0}$), represented in Eq. (3) [2–5,12,19,20,22–24]:

$$\Gamma = 3A_g + 5A_u + 5B_g + 3B_u + 5E_g + 5E_u \quad (3)$$

For only Raman and IR-active modes, the vibration are reduced to

$$\Gamma = 3A_g + 4A_u + 5B_g + 5E_g + 4E_u \quad (4)$$

The $3A_g$, $5B_g$ and $5E_g$ modes are Raman-active, and the $4A_u$ and $4E_u$ modes are IR-active. The $1A_u$ and $1E_u$ correspond to the zero frequency of acoustic modes. The $3B_u$ modes are silent. The A and B modes are nondegenerate, and the E mode is doubly degenerate. The "g" and "u" subscripts indicate the parity

Table 1
Lattice parameters of the products.

Lattice parameter	$CaMoO_4$	$SrMoO_4$	$CaWO_4$	$SrWO_4$
a (Å)	5.2172	5.4103	5.2560	5.4202
c (Å)	11.4201	12.0673	11.4007	12.0031

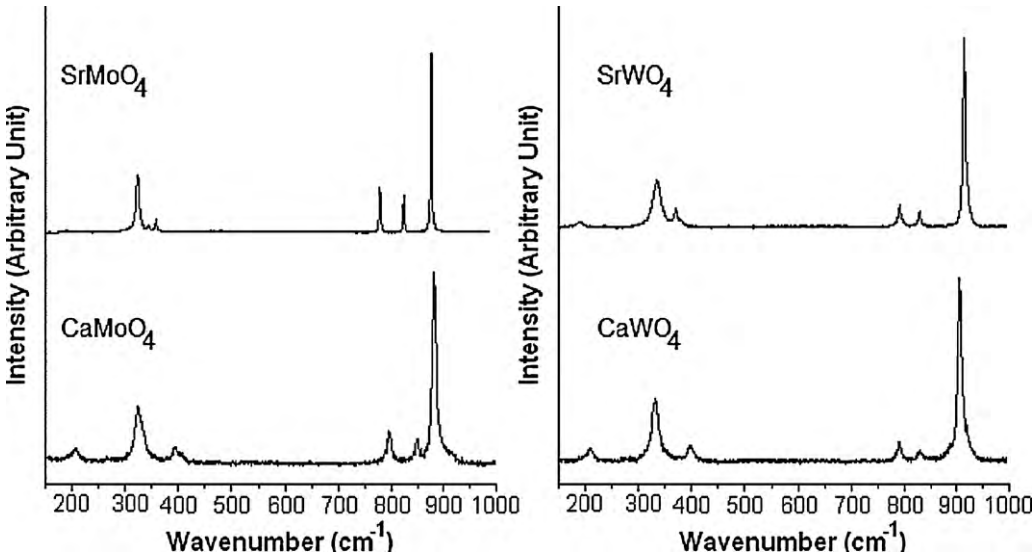

Fig. 2. Raman spectra of $CaMoO_4$, $SrMoO_4$, $CaWO_4$ and $SrWO_4$.

under inversion in centrosymmetric crystals. The A_g, B_g and E_g modes arise from the same motion of MXO_4. Thus, the 13 zone-center Raman-active modes are expected, presented by Eq. (5) [3–6,19,20,22–24]:

$$\Gamma = 3A_g + 5B_g + 5E_g \quad (5)$$

The Raman vibrational modes can be classified into two groups – the external and internal modes. The first is known as lattice phonon, corresponding to the motion of M^{2+} cations relative to the rigid $[XO_4]^{2-}$ tetrahedron units. The second belongs to the vibration inside $[XO_4]^{2-}$ tetrahedron units, and is considered as the stationary state of mass center. In free space, $[XO_4]^{2-}$ tetrahedrons have T_d symmetry [6,23,24], and are composed of four internal modes ($\nu_1(A_1)$, $\nu_2(E_1)$, $\nu_3(F_2)$ and $\nu_4(F_2)$), one free rotation mode ($\nu_{f.r.}(F_1)$) and one translation mode (F_2) [1,3–6,19,20,22–24]. When $[XO_4]^{2-}$ tetrahedrons reside in scheelite structure, the point symmetry is reduced to S_4 [5,23,24]. Raman spectra, recorded on 150–1000 cm^{-1}, are shown in Fig. 2, and their six vibrations are summarized in Table 2. Raman wavenumbers shifted from $CaMoO_4$ to $CaWO_4$ and $SrMoO_4$ to $SrWO_4$, caused by the covalent bond formation between the Mo^{6+} (or W^{6+}) and O^{2-} ions in the $[MoO_4]^{2-}$

Table 2
Raman wavenumbers of the products.

Lattice vibration	Wavenumber (cm^{-1})			
	$CaMoO_4$	$SrMoO_4$	$CaWO_4$	$SrWO_4$
$\nu_1(A_g)$	907	915	873	883
$\nu_3(B_g)$	845	842	832	831
$\nu_3(E_g)$	795	795	792	794
$\nu_4(B_g)$	400	371	392	368
$\nu_2(A_g)$	333	335	322	327
$\nu_{f.r.}(A_g)$	208	189	203	181

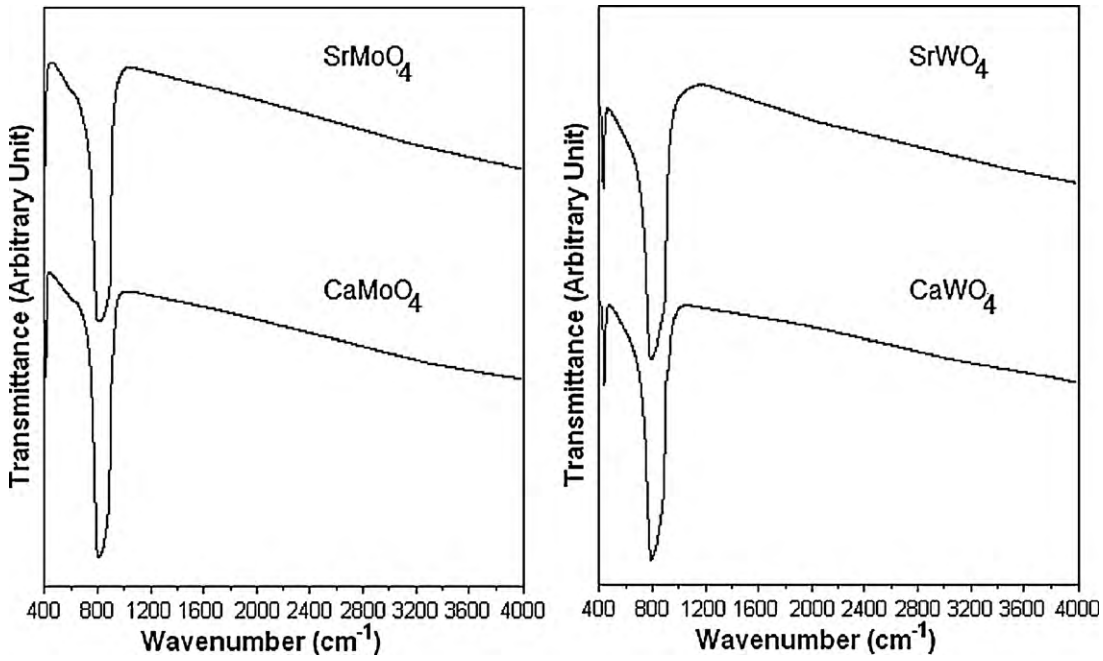

Fig. 3. FTIR spectra of $CaMoO_4$, $SrMoO_4$, $CaWO_4$ and $SrWO_4$.

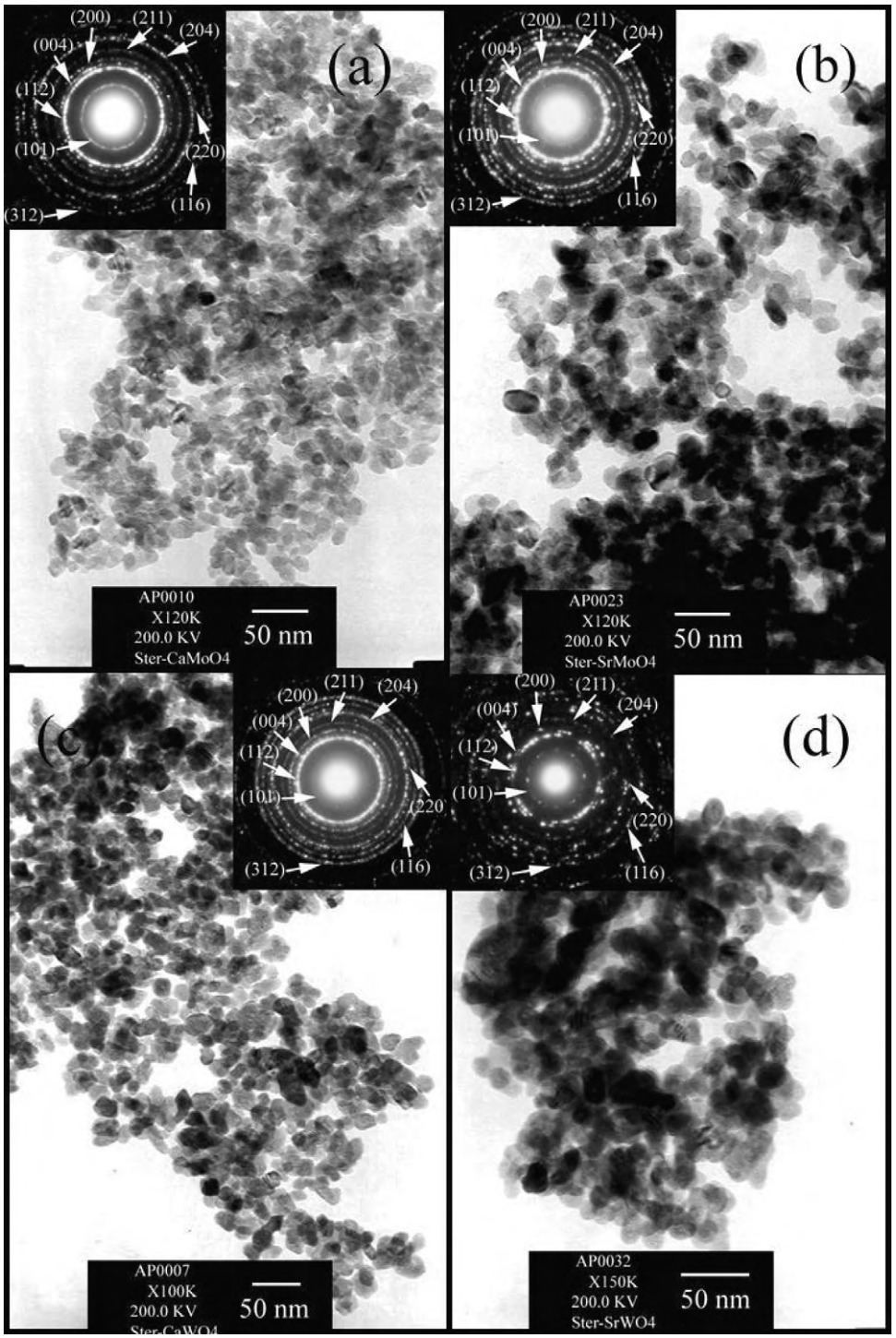

Fig. 4. TEM images and SAED patterns of (a–d) $CaMoO_4$, $SrMoO_4$, $CaWO_4$ and $SrWO_4$, respectively.

and $[WO_4]^{2-}$ complexes, which change the efficient mass of the oscillating atoms [25].

The internal $\nu_3(F_2)$ stretching and $\nu_4(F_2)$ bending modes are actives in only IR frequencies. In fact, the stretching modes arise from X–O anti-symmetric stretching vibrations in the $[XO_4]^{2-}$ tetrahedron groups [1,3,4]. The FITR spectra of nanoparticles at the wavenumber range of 400–4000 cm^{-1} are shown in Fig. 3. The strong X–O stretching vibration was detected as strong Mo–O stretching at 737–974 and 720–970 cm^{-1} and weak Mo–O bending at 423 and 411 cm^{-1} for $CaMoO_4$ and $SrMoO_4$, and strong W–O stretching at 657–966 and 648–950 cm^{-1} and weak W–O bending at 461 and 434 cm^{-1} for $CaWO_4$ and $SrWO_4$ [20], respectively.

TEM images (Fig. 4) present all product morphologies, which have good narrow particle-sized distributions containing a number of round nanoparticles with uniform sizes, which improve their luminescent properties. The nanoparticle sizes were measured from the TEM images, of which the size-distributions are narrow and very close to normal curves, as shown in Fig. 5. The average particle size and standard deviation of these products are 12.06 ± 1.65, 16.40 ± 2.44, 15.49 ± 2.19, and 15.40 ± 2.30 nm for

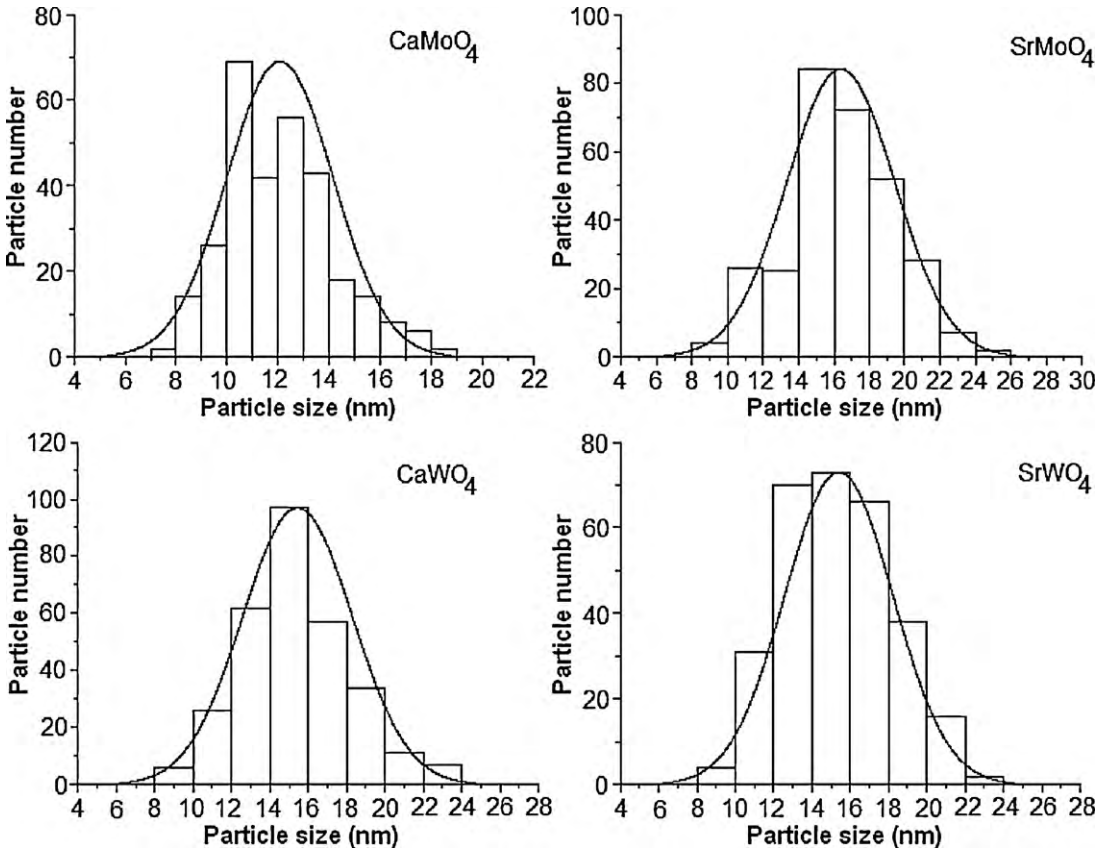

Fig. 5. Particle-sized distribution curves of $CaMoO_4$, $SrMoO_4$, $CaWO_4$ and $SrWO_4$.

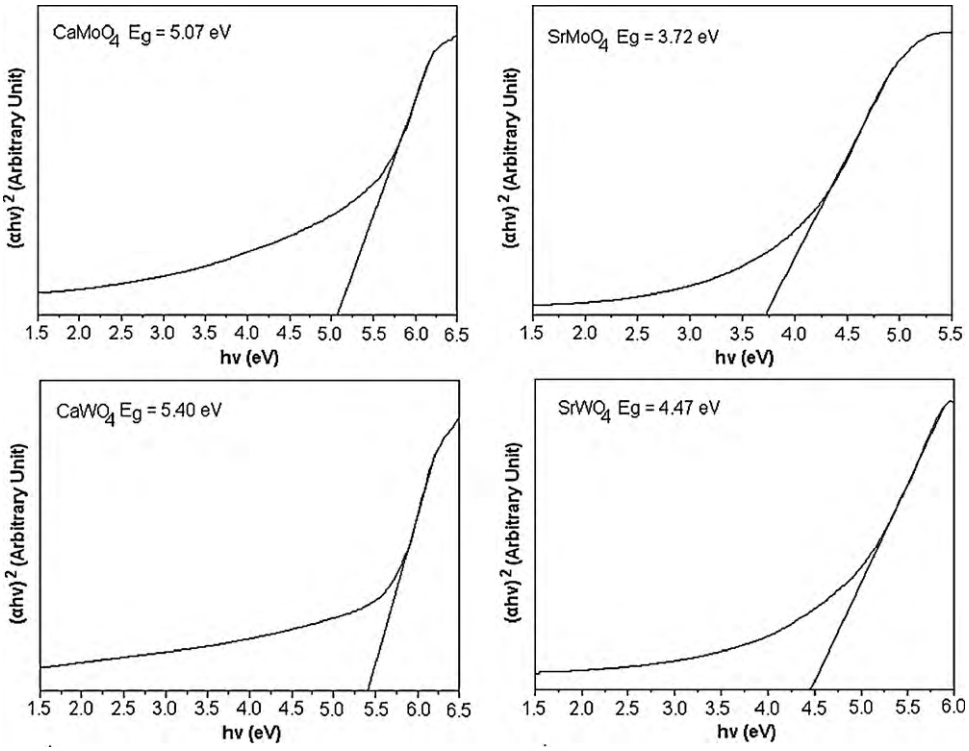

Fig. 6. The $(\alpha h\nu)^2$ vs $h\nu$ plots of $CaMoO_4$, $SrMoO_4$, $CaWO_4$ and $SrWO_4$.

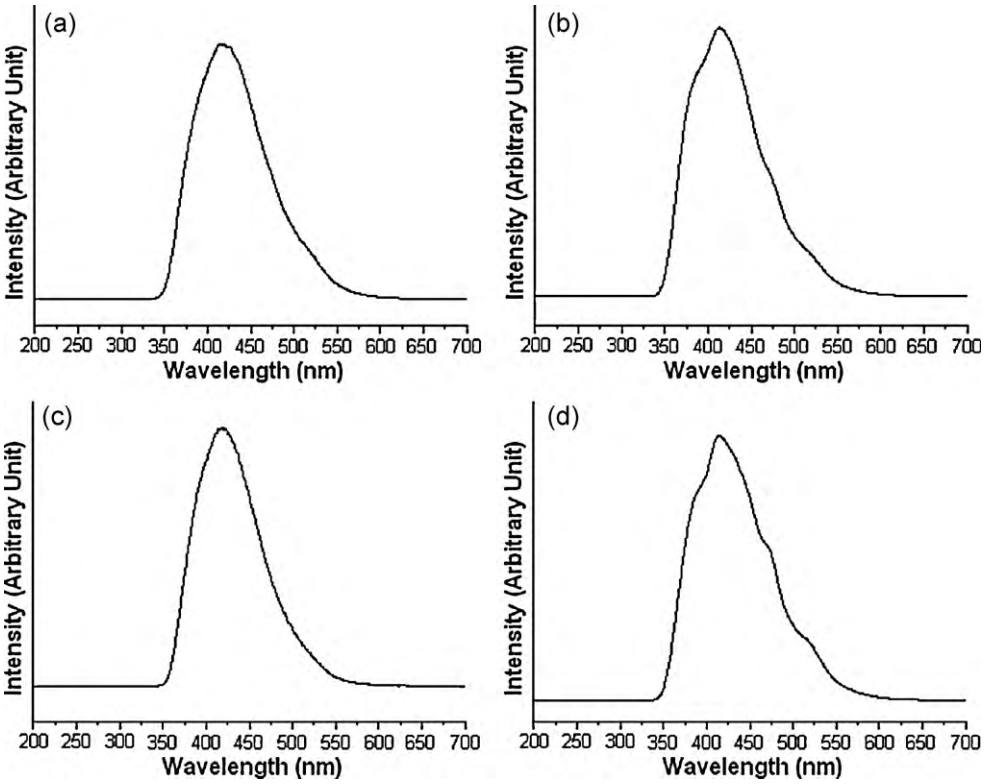

Fig. 7. PL spectra of (a–d) $CaMoO_4$, $SrMoO_4$, $CaWO_4$, and $SrWO_4$, respectively.

$CaMoO_4$, $SrMoO_4$, $CaWO_4$ and $SrWO_4$, respectively. SAED patterns (inserted in TEM images) shape like fully concentric rings, implying that the products were polycrystalline. The interplanar spaces were calculated from the diameters of the rings, and compared with those of the JCPDS standard [17]. All SAED patterns show the same (1 0 1), (1 1 2), (0 0 4), (2 0 0), (2 1 1), (2 0 4), (2 2 0), (1 1 6) and (3 1 2) planes – in good accordance with the XRD results.

Fig. 6 shows the $(\alpha h\nu)^2$ vs $h\nu$ curves of $CaMoO_4$, $SrMoO_4$, $CaWO_4$ and $SrWO_4$, which were calculated from their UV–visible absorbance using the equation proposed by Wood and Tauc – shown in Eq. (6) [2,12,19] below.

$$\alpha h\nu = (h\nu - E_g)^n \quad (6)$$

where α is the absorbance, h the Planck constant, ν the photon frequency, E_g the energy gap, and n the pure numbers associated with the different types of electronic transitions. For $n = 1/2$, 2, 3/2 and 3, the transitions are the direct allowed, indirect allowed, direct forbidden, and indirect forbidden, respectively. Each energy gap was determined by extrapolation of each linear portion of the curves to $\alpha = 0$. In the present research, the molybdates and tungstates with scheelite-type tetragonal structure present the direct allowed electronic transition ($n = 1/2$) [2,12,26], and the energy gaps of $CaMoO_4$, $SrMoO_4$, $CaWO_4$ and $SrWO_4$ are 5.07, 3.72, 5.40 and 4.47 eV, respectively. They are in good accordance with the previous reports [5,19,26–28]. In fact, energy band gap depends on several factors such as the electronegativity of transition metal ions, connectivity of the polyhedrons, deviation in the O–X–O bonds, distortion of the $[XO_4]^{2-}$ tetrahedrons, growth mechanism, and degree of structural order–disorder in the lattice [2,19].

Generally, the emission phenomena of metal molybdates and tungstates occur by the electronic charge transfer within the $[XO_4]^{2-}$ units. The hybridization of the molecular orbital of $[XO_4]^{2-}$ complexes was caused by the coupling between the O2p(σ) and O2p(π) ligand orbitals and Mo4d(t_2) and Mo4d(e) orbitals for metal molybdates, or W5d(t_2) and W5d(e) orbitals for metal tungstates. The four ligand p(σ) orbitals are compatible with the tetrahedral representation for the a_1 and t_2 symmetries, and the eight ligand p(π) orbitals are for the t_1, t_2 and e symmetries. The top occupied state has t_1 symmetry formed from O2p(π) states. The lowest unoccupied state has e symmetry formed from a combination of the Mo4d(e) and O2p(π) orbitals for metal molybdates, and W5d(e) and O2p(π) orbitals for metal tungstates, to give anti-bonding (*). The hybridizations between the Mo4d for metal molybdates or W5d for metal tungstates and O2p orbitals are specified as covalent bonding between the ions. For ground state system, all one-electron states below band gap (E_g) are filled to give a many-electron $^1A_1$ state. At the lowest excited state, there are one hole in the t_1 (primarily O2p(π)) state and one-electron in the e (primarily Mo4d for metal molybdates, and W5d for metal tungstates) state which give rise to many-electron $^1T_1$, $^3T_1$, $^1T_2$ and $^3T_2$ states. Only $^1T_2 \rightarrow {}^1A_1$ is the probable or allowed transition [20,22–24].

Fig. 7 shows photoluminescence (PL) spectra at room temperature of $CaMoO_4$, $SrMoO_4$, $CaWO_4$ and $SrWO_4$ using the excitation wavelengths of 212, 290, 214, and 276 nm, respectively. These spectra are rather broad covering the 350–600 nm range. Multi-peaks of emission spectra were specified using Gaussian analysis in combination with the origin program. They exhibited the emission peaks at 414, 413, 418, and 414 nm for $CaMoO_4$, $SrMoO_4$, $CaWO_4$ and $SrWO_4$, respectively – in accordance with the emissions of previous reports [7,8,10,11,27,29]. It is generally known that the emission spectra of the metal molybdates and tungstates are mainly influenced by charged transitions within the $[XO_4]^{2-}$ complexes, including several factors such as distortions of the $[XO_4]^{2-}$ tetrahedron groups caused by the different angles of O–X–O, particle sizes, crystalline degree, morphology and surface defects.

4. Conclusions

Alkaline earth metal molydate and tungstate (M = Ca and Sr) nanoparticles were successfully synthesized by the co-

precipitation process. It is a simple method, low energy consumption and friendly to the environment. XRD and SAED patterns show that all products are body-centered tetragonal scheelite structure. Their vibrations were studied by Raman and FTIR spectroscopy, of which the results are in accordance with the XRD and SAED analyses. TEM revealed the morphologies of the products which show the nanosized particles with narrow normal distributions. The direct allowed energy gaps of $CaMoO_4$, $SrMoO_4$, $CaWO_4$ and $SrWO_4$, determined using Wood and Tauc method, are 5.07, 3.72, 5.40, and 4.47 eV, respectively.

Acknowledgement

This research was supported by the National Nanotechnology Center (NANOTEC), a member of National Science and Technology Development Agency (NSTDA), Ministry of Science and Technology, Thailand.

References

[1] A. Phuruangrat, T. Thongtem, S. Thongtem, J. Ceram. Soc. Jpn. 116 (2008) 605–609.
[2] L.S. Cavalcante, J.C. Sczancoski, R.L. Tranquilin, M.R. Joya, P.S. Pizani, J.A. Varela, E. Longo, J. Phys. Chem. Solid 69 (2008) 2674–2680.
[3] L.S. Cavalcante, J.C. Sczancoski, J.W.M. Espinosa, J.A. Varela, P.S. Pizani, E. Longo, J. Alloy Compd. 474 (2009) 195–200.
[4] L.S. Cavalcante, J.C. Sczancoski, L.F. Lima Jr., J.W.M. Espinosa, P.S. Pizani, J.A. Varela, E. Longo, Cryst. Growth Des. 9 (2009) 1002–1012.
[5] J.C. Sczancoski, L.S. Cavalcante, M.R. Joya, J.A. Varela, P.S. Pizani, E. Longo, Chem. Eng. J. 140 (2008) 632–637.
[6] T. Thongtem, A. Phuruangrat, S. Thongtem, Mater. Lett. 62 (2008) 454–457.
[7] J. Liu, J. Ma, B. Lin, Y. Ren, X. Jiang, J. Tao, X. Zhu, Ceram. Int. 34 (2008) 1557–1560.
[8] L. Sun, M. Cao, Y. Wang, G. Sun, C. Hu, J. Cryst. Growth 289 (2006) 231–235.
[9] Z. Lou, M. Cocivera, Mater. Res. Bull. 37 (2002) 1573–1582.
[10] D. Chen, G. Shen, K. Tang, H. Zheng, Y. Qian, Mater. Res. Bull. 38 (2003) 1783–1789.
[11] J. Liao, B. Qiu, H. Wen, J. Chen, W. You, L. Liu, J. Alloy Compd. 487 (2009) 758–762.
[12] J.C. Sczancoski, M.D.R. Bomio, L.S. Cavalcante, M.R. Joya, P.S. Pizani, J.A. Varela, E. Longo, M.S. Li, J.A. Andrés, J. Phys. Chem. C 113 (2009) 5812–5822.
[13] J.H. Ryu, J.W. Yoon, C.S. Lim, W.C. Oh, K.B. Shim, J. Alloy Compd. 390 (2005) 245–249.
[14] T. Thongtem, A. Phuruangrat, S. Thongtem, J. Ceram. Proc. Res. 9 (2008) 258–261.
[15] L.S. Cavalcante, J.C. Sczancoski, R.L. Tranquilin, J.A. Varela, E. Longo, M.O. Orlandi, Particuology 7 (2009) 353–362.
[16] T. Thongtem, A. Phuruangrat, S. Thongtem, J. Ceram. Proc. Res. 9 (2008) 189–191.
[17] Powder Diffract. File, JCPDS-ICDD, 12 Campus Boulevard, Newtown Square, PA 19073-3273, U.S.A., 2001.
[18] C. Suryanarayana, M.G. Norton, X-ray Diffraction. A Practical Approach, Plenum Press, NY, 1998.
[19] J.C. Sczancoski, L.S. Cavalcante, M.R. Joya, J.W.M. Espinosa, P.S. Pizani, J.A. Varela, E. Longo, J. Colloid Interface Sci. 330 (2009) 227–236.
[20] A. Phuruangrat, T. Thongtem, S. Thongtem, J. Alloy Compd. 481 (2009) 568–572.
[21] F.Q. Dong, Q.S. Wu, Y.P. Ding, J. Alloy Compd. 476 (2009) 571–574.
[22] A. Phuruangrat, T. Thongtem, S. Thongtem, J. Cryst. Growth 311 (2009) 4076–4081.
[23] T. Thongtem, A. Phuruangrat, S. Thongtem, Appl. Surf. Sci. 254 (2008) 7581–7585.
[24] T. Thongtem, S. Kaowphong, S. Thongtem, Appl. Surf. Sci. 254 (2008) 7765–7769.
[25] T.T. Basiev, A.A. Sobol, Y.K. Voronko, P.G. Zverev, Opt. Mater. 15 (2000) 205–216.
[26] M.A.M.A. Maurera, A.G. Souza, L.E.B. Soledade, F.M. Pontes, E. Longo, E.R. Leite, J.A. Varela, Mater. Lett. 58 (2004) 727–732.
[27] J.H. Ryu, B.G. Choi, J.W. Yoon, K.B. Shim, K. Machi, K. Hamada, J. Lumin. 124 (2007) 67–70.
[28] R. Lacomba-Perales, J. Ruiz-Fuertes, D. Errandonea, D. Martínez-García, A. Segura, Europhys. Lett. 83 (2008) (arti. no. 37002).
[29] Z. Chen, Q. Gong, J. Zhu, Y.P. Yuan, L.W. Qian, X.F. Qian, Mater. Res. Bull. 44 (2009) 45–50.